AGU PUBLICATIONS

JGR

Journal of Geophysical Research: Oceans

RESEARCH ARTICLE

10.1002/2016JC012284

Key Points:
- Wind driven circulation in a peri alpine lake surrounded by complex orography which affects the wind distribution over the lake surface
- Peculiar superstreaks are reproduced in the interior of the lake together with upwelling and downwelling regions along the coastline
- The eddy viscosities showed substantial differences with respect to the ocean case

Correspondence to:
M. A. Santo,
marcoantonio.santo@phd.units.it

Citation:
Santo, M. A., M. Toffolon, G. Zanier, L. Giovannini, and V. Armenio (2017), Large eddy simulation (LES) of wind-driven circulation in a peri-alpine lake: Detection of turbulent structures and implications of a complex surrounding orography, *J. Geophys. Res. Oceans*, *122*, doi:10.1002/2016JC012284.

Received 31 AUG 2016
Accepted 5 MAY 2017
Accepted article online 15 MAY 2017

Large eddy simulation (LES) of wind-driven circulation in a peri-alpine lake: Detection of turbulent structures and implications of a complex surrounding orography

Marco A. Santo[1], Marco Toffolon[2], Giulia Zanier[3], Lorenzo Giovannini[2], and Vincenzo Armenio[1]

[1]Department of Engineering and Architecture, University of Trieste, Trieste, Italy, [2]Department of Civil, Environmental and Mechanical Engineering, University of Trento, Trento, Italy, [3]Iefluids s.r.l., Trieste, Italy

Abstract We investigate wind-driven circulation in a peri-alpine lake (Lake Ledro - Italy) using LES-COAST. Lake Ledro is interesting because its own dimensions are suited for LES and it is surrounded by complex orography, affecting wind distribution. We consider the winter condition when stratification is nearly absent. Two types of time-varying wind stress are used: spatially homogeneous and spatially inhomogeneous respectively. The analysis of the eddy viscosities shows substantial differences with respect to the ocean case characterized by absence of coastal boundaries and homogeneous, steady wind. The quantities exhibit a noticeable inhomogeneous behavior: the horizontal eddy viscosity is larger in the water body far from the boundaries, whereas the vertical one is larger close to the lateral boundaries due to the presence of a boundary layer. The energetic bottom boundary layer, typically occurring in lakes, is not present. This because of the intrinsic unsteadiness of the thermal wind blowing over the lake and due to the absence of large amplitude internal waves, the latter present only in case of stable stratification. In the inhomogeneous wind case, up-welling and down-welling areas are not confined along the shoreline only, but are also generated in the water body due to substantial horizontal velocity divergence, and turbulent mixing, quantified by eddy viscosities, TKE and its dissipation rate, appears enhanced with respect to the homogeneous wind case. Finally, downwelling/upwelling areas along the windward/leeward coastline respectively were observed, whose quantitative estimation may give explanation for the bloom of cyanobacteria at the lake surface observed in winter.

1. Introduction

Lakes and reservoirs are complex systems where transport of substances (oxygen, nutrients, pollutants) and heat (affecting the thermal stratification) depends on slow flows. The primary source of momentum is the wind stress on the water surface, so that mixing is effective in the surface layer, while the interior remains relatively calm [e.g., *Wüest and Lorke*, 2003]. Mixing is further inhibited in presence of a strong density stratification, which can reduce the exchanges across the pycnocline even to molecular diffusion rates. In this context, convective flows and large scale turbulent structures are important because they effectively contribute to the vertical transport by means of local downwelling and upwelling phenomena.

Modeling turbulence in lentic systems is indeed a complicated issue. Standard applications rely on Reynolds Averaged Navier-Stokes (RANS) equations, possibly including transport equations for the turbulent kinetic energy and its dissipation rate (e.g., k-ϵ models). In case of small basins, rotation and topographic effects, together with the unsteady wind-driven source of momentum, make difficult the calibration of large scale circulation models. This is even more true in case of stable/unstable temperature stratification complicated by the presence of heat exchange at the free surface. Recently, for the mentioned reasons the use of eddy-resolving models has been encouraged (for a discussion, see *Burchard et al.* [2008]). While direct numerical simulations (DNS) of the Navier-Stokes equations are unfeasible due to a nonaffordable computational cost (for a discussion, see *Piomelli* [1999]), large eddy simulation (LES) has proved to be a good candidate to solve fluid dynamic problems characterized by complex physics and geometry. In LES the large scales of turbulence, more anisotropic and energetic, are solved directly through a three-dimensional (3D) unsteady simulation, while the small scales, which are dissipative and characterized by a more universal behavior, are

modeled by using a subgrid scale (SGS) model. LES has been widely used to simulate complex flows of interest to environmental fluid mechanics, whose accurate reproduction is not straightforward using standard RANS-like methodologies [*Sarkar and Armenio*, 2013].

Very few examples are present in literature where LES has been used to study hydrodynamic processes in lakes or coastal basins. LES was used to understand processes involved in sidearms of lakes due to thermal forcing in absence of wind [*Dittko et al*., 2013], and to investigate fundamental processes occurring in real scale basins but referring to simple rectangular domains [*Sander et al*., 2000; *Scalo et al*., 2013; *Mironov et al*., 2002]. Recently, an eddy-resolving LES model (LES-COAST) has been developed to simulate the hydrodynamics within full-scale closed or semiclosed coastal basins [*Roman et al*., 2010]. Some details on the model are reported in section 2. The model was successfully used to reproduce wind-driven circulations in the industrial harbour of Trieste (Italy) [*Petronio et al*., 2013] and in the Barcelona harbour (Spain) under typical meteorological conditions [*Galea et al*., 2014].

LES-COAST has been applied to study coastal areas, considering a constant unidirectional and homogeneous wind stress at the air-water surface. In *Petronio et al*. [2013], the effect of ships and anthropogenic structures on the wind distribution within the bay was considered through empirical formulas aimed at reducing the wind stress in regions of intense recirculations. However, such approach is not appropriate for lakes where the surrounding orography is complex and the wind field is strongly inhomogeneous [*Laval et al*., 2003; *Rueda et al*., 2005]. In fact, lakes located in mountainous regions can be exposed to thermally-driven atmospheric circulations. They develop especially in clear-sky days and mark the local wind climatology with a pronounced daily periodicity, as their direction regularly reverses between day and night [*Serafin and Zardi*, 2010; *Rampanelli et al*., 2004]. Thermally-driven circulations may be enhanced by local orography and may develop at a valley scale (up-valley during the day and down-valley at night) and/or at smaller scales, influencing only a slope of the valley and, hence, a portion of the lake. As a consequence, wind data obtained from observations at a single location over the lake surface may be not representative of the actual spatial distribution of the wind speed and direction over the lake. In these cases, fine-resolution meteorological simulations are needed to properly take into account the mechanical effects of the topography on the wind field and to adequately simulate the development of thermally-driven local circulations.

In the present paper we study the wind-driven circulation in a lake using LES-COAST and considering the actual geometric features of the lake and of the surrounding. First we use a spatial homogeneous wind field, varying in time according to the data recorded by a meteorological station located at the center of the lake (Figure 1a); then we use the realistic wind forcing obtained from high-resolution inhomogeneous and time-dependent wind fields simulated by means of the atmospheric Weather Research and Forecasting model (WRF), a well-known meteorological model which can be applied to study sites with small horizontal and vertical dimensions in complex terrain [*Papanastasiou et al*., 2010; *Arrilaga et al*., 2016].

As regards the site, among the others, Lake Ledro (northern Italy, see Figure 1) is suited to be studied with a LES model for three main reasons: Its own dimensions are appropriate for an eddy resolving LES, the surface area and the maximum depth being respectively 2.1 km^2 and 48 m; Recently it has been subject to abundant blooms of the harmful cyanobacterium *Planktothrix rubescens* under weakly stratified conditions [*Barbato*, 1977], similar to what happened in other sub-alpine lakes in Europe [*Salmaso et al*., 2006; *D'Alelio and Salmaso*, 2011]; It is located at 652 a.s.l. in a valley surrounded by a complex orography with peaks reaching 1988 m a.s.l. Therefore the local orographic features channel the wind to certain directions [*Laiti et al*., 2014; *Giovannini et al*., 2015] and, together with vegetation canopy or anthropogenic structures, affect the wind distribution [*Laval et al*., 2003; *Rueda et al*., 2005], resulting in peculiar lake circulations [*Podsetchine and Schernewski*, 1999; *Rubbert and Köngeter*, 2005; *Toffolon and Rizzi*, 2009].

Here we reproduce a winter case where thermal stratification is nearly absent. This is known as a typical period for *P. rubescens* to emerge at the lake surface. To this aim, we selected the week 16–22 January 2012, when the maximum temperature difference along the water column was less than 0.4°C and the latent heat fluxes that could give rise to convection are low, thus allowing us to neglect buoyancy effects on lake hydrodynamics as a first case study. The aim is to improve the knowledge of the gross circulation as well as of large-scale turbulent structures that develop in complex lakes, and to detect the processes that facilitate the upwelling of the toxic cyanobacterium up to the lake surface.

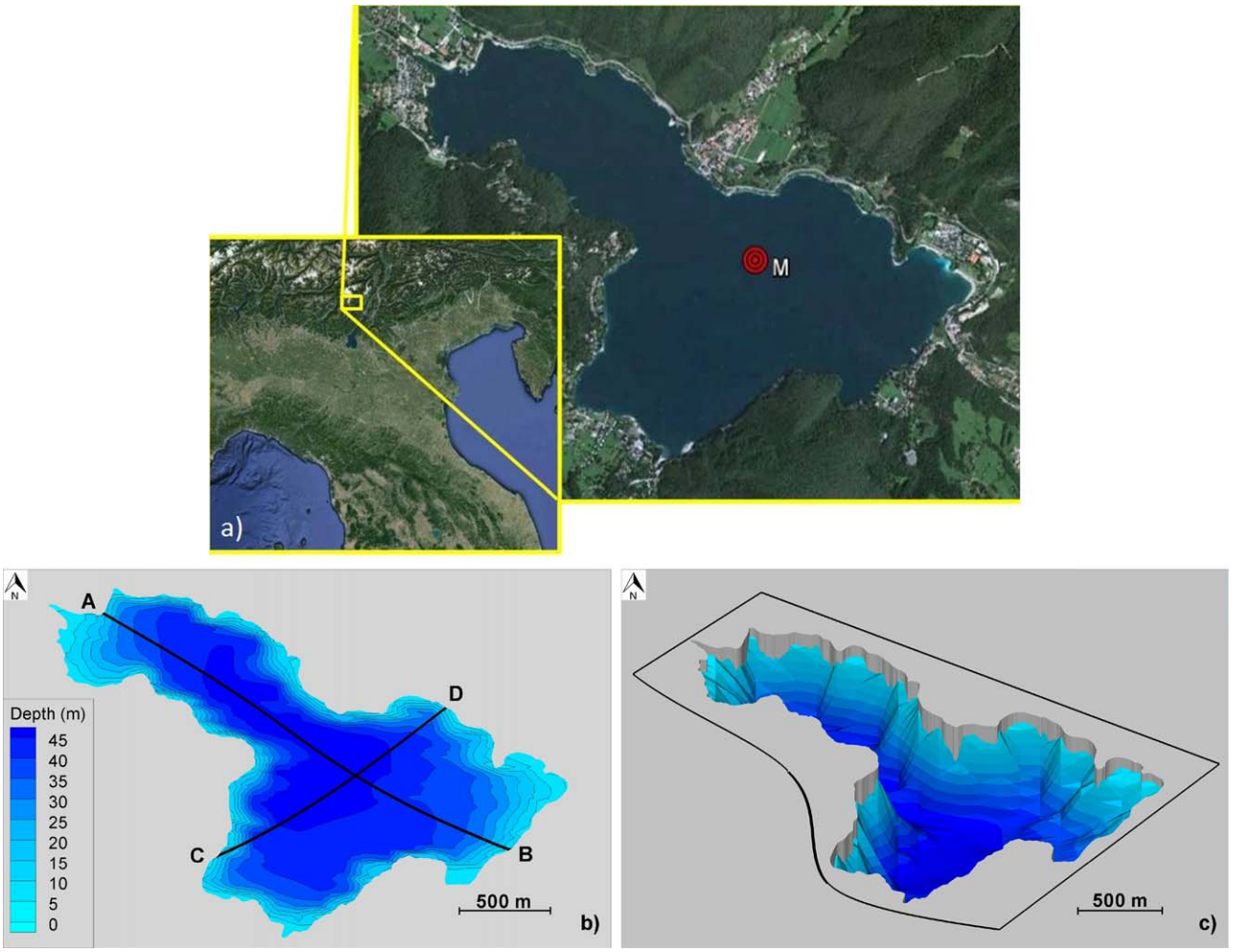

Figure 1. Position and bathymetry of Lake Ledro: (a) satellite image and location, the red point indicates the position of the platform hosting the meteorological station; (b) depth contours and main axes AB and CD; (c) bathymetry reconstructed by the Immersed Boundary Method (IBM), showing the edge of the curvilinear computational domain (in black), the rigid bodies of shoreline (in grey) and bathymetry (blue). The vertical dimension in Figure 1c is increased by a factor 500 with respect to the horizontal axes. Hereafter the same distortion rate is applied in the other figures.

We are aware that important dynamics, associated to the presence of temperature stratification cannot be exploited in the present study. However here we exploit hydrodynamic features occurring in realistic situations of neutral stratification; also, the results of the present study will constitute an important starting point for the ongoing study of the stratified situation. The latter is the topic of a successive paper.

The paper is structured as follows. Section 2 presents the case study, describes the main features of LES-COAST and reports the characteristics of the meteorological simulation. Results are discussed in section 3 for an idealized case where the wind is considered homogeneous over the surface of the lake. Results for the realistic case of inhomogeneous wind forcing are in section 4. Finally, in section 5 concluding remarks are given.

2. The Mathematical Formulation

The study is carried out numerically, using the eddy-resolving model LES-COAST. It solves the three-dimensional Boussinesq form of the nonhydrostatic, filtered Navier-Stokes equations [*Petronio et al*., 2013]:

$$\frac{\partial \bar{u}_i}{\partial x_i} = 0\,, \tag{1}$$

$$\frac{\partial \bar{u}_i}{\partial t}+\frac{\partial \bar{u}_i\bar{u}_j}{\partial x_j}=-\frac{1}{\rho_0}\frac{\partial \bar{p}}{\partial x_i}+\nu\frac{\partial^2 \bar{u}_i}{\partial x_j\partial x_j}-2\epsilon_{ijk}\Omega_j\bar{u}_k-\frac{\bar{\rho}}{\rho_0}g_i\delta_{i3}-\frac{1}{\rho_0}\frac{\partial \tau_{ij}}{\partial x_j}\,, \tag{2}$$

where u_i, Ω_i and g_i are the i-th components of velocity, Earth rotation rate and gravitational acceleration vectors, respectively; ϵ_{ijk} and δ_{ij} are the Levi-Civita and Kronecker symbol respectively, p is the hydrodynamic pressure, ν the kinematic viscosity and ρ is the density of the water (with ρ_0 a reference value). Here we denote with u_1, u_2, u_3 or u, v, w the velocity components along x_1, x_2, x_3 or x, y, z axes. The frame of reference has the origin over the free surface of the lake, x_1, x_2 over the horizontal plane and x_3 pointing upward.

The overbar refers to the filtering operation needed to separate the resolved scales from the unresolved ones ($u_i=\bar{u}_i+u_{i,sgs}$ with $u_{i,sgs}$ the velocity field removed by the filter operation). Filtering is performed implicitly in the real space through a top-hat filter function proportional to the length of the grid cells. The filtering operation applied to the nonlinear term of the NS equations introduces the SGS stresses $\tau_{ij}=\rho_0(\overline{u_iu_j}-\bar{u}_i\bar{u}_j)$ representing the effect of the unresolved fluctuations over the resolved field. In the classic Smagorinsky model [*Smagorinsky*, 1963] the SGS stresses are related to the resolved strain rate tensor $\bar{S}_{ij}$ through a SGS eddy viscosity ν_τ as follows:

$$\frac{1}{\rho_0}\left(\tau_{ij}-\frac{\delta_{ij}}{3}\tau_{kk}\right)=-2\nu_\tau\bar{S}_{ij}\,,\quad \bar{S}_{ij}=\frac{1}{2}\left(\frac{\partial \bar{u}_i}{\partial x_j}+\frac{\partial \bar{u}_j}{\partial x_i}\right). \tag{3}$$

The turbulent eddy-viscosity, ν_τ, is modeled as a characteristic velocity scale multiplied by a length scale proportional to $\sqrt[3]{\Delta_x\Delta_y\Delta_z}$, Δx_i being the cell dimension in the i-direction. In the case of coastal areas, as well as for lakes, finding a unique length scale representative of the three dimensions of the cells could lead to an overestimation of the eddy viscosity in all directions because of the strong anisotropy of the cells used to discretize the domain.

In order to overcome this problem we adopt the ASM developed by *Roman et al*. [2010]. The model uses a two-SGS-eddy-viscosity concept. The quantities are defined as:

$$\nu_{\tau,H}=(C_HL_H)^2\,|\bar{S}_H|\,, \tag{4}$$

$$\nu_{\tau,V}=(C_VL_V)^2\,|\bar{S}_V|\,, \tag{5}$$

where $L_H=\sqrt{\Delta_x{}^2+\Delta_y{}^2}$ and $L_V=\Delta_z$, and

$$|\bar{S}_H|=\sqrt{2\bar{S}_{11}^2+2\bar{S}_{22}^2+4\bar{S}_{12}^2}\,, \tag{6}$$

$$|\bar{S}_V|=\sqrt{4\bar{S}_{13}^2+2\bar{S}_{33}^2+4\bar{S}_{23}^2}\,. \tag{7}$$

In the equations above, the subscripts V and H stand for vertical and horizontal respectively. The calibration of the empirical constants C_V and C_H was carried out in *Roman et al.* [2010]. They simulated a standard turbulent-plane Poiseuille flow with increasing grid anisotropy, quantified through the grid aspect-ratio $\sqrt{\Delta_x^2+\Delta_y^2}/\Delta_z$ (with $\Delta_x\sim\Delta_y$), and compared the results with reference experimental and benchmark numerical data. In our case (sections 3 and 4) the average aspect ratio is $\sim$10, a value for which $C_H=0.028$ and $C_V=0.3$ [*Roman et al*., 2010].

This work has to be considered as part of a broader analysis, in which the effects of stratification on the hydrodynamics will be modeled via LES methodology; for this reason in the present analysis we study the case of neutral stratification to be taken as informative for the study as a whole. Thus, we do not need to solve any active scalar equation (i.e., for temperature, salinity, sediment concentration, etc.) and to include the terms representing the buoyancy force in equation (2). Conversely, although the dimension of the Lake Ledro is small, the effect of Earth rotation has to be taken into account especially during the morning when the wind speed and the consequent velocities at the surface are small. This will be discussed in section 3.1.

Every single feature composing LES-COAST, namely, Immersed Boundary Method (IBM), wall-layer model, SGS model and synthetic turbulence at the inlet boundaries have been extensively validated against test cases where either numerical or experimental data were available [see *Roman et al*., 2009a,2009b,2010; *Petronio et al*., 2013]. LES-COAST has been used to study mixing and water renewal in a number of sites. In the

analysis of hydrodynamics in the Muggia bay [*Petronio et al*., 2013] a good agreement was found between numerical velocity profiles and field data at significant locations. In *Galea et al*. [2014], the model was applied to study mixing in the Barcelona harbor. Also in this latter case, the velocity profiles obtained with LES-COAST were in very good agreement with those measured in the harbor.

2.1. Computational Domain and Boundary Conditions

Lake Ledro has an irregular shape difficult to reproduce numerically using structured-grid solvers. Here we use a mixed approach which takes advantage of the curvilinear grids for reproducing the gross structure of the bathymetry and of IBM for the details hardly reproducible using curvilinear structured grids.

Figure 1c depicts the shoreline and the bathymetry. A curvilinear grid (whose upper boundary lines are depicted in black) was generated and the immersed boundaries were introduced to reproduce the actual bathymetry. There, a fictitious body force was implemented in the momentum equation mimicking the effect of the solid boundaries. This methodology, initially designed for orthogonal grids, was adapted to the curvilinear coordinates by *Roman et al*. [2009b].

For the present study, the computational domain was discretized into 256 cells along the north-west/south-east direction (parallel to axis AB in Figure 1b), 128 cells along the north-east/south-west direction (parallel to axis CD), and 32 cells along the vertical. The grid was uniform along the three dimensions, curvilinear in the horizontal planes and orthogonal along the vertical. The cell size was of about 12 m in the horizontal direction and 1.3 m along the vertical. This is typical of high Reynolds number LES where the near wall dynamics is parametrized by the use of wall-layer models.

At the solid walls we use the wall-layer model developed by *Roman et al*. [2009a] which is based on the evaluation of a near-wall eddy viscosity whose value is calculated assuming that the velocity profile has a logarithm shape. Two different values are adopted to model roughness. In order to reproduce the effect of different sediment types and vegetation, we set the littoral and bottom roughness equal to 0.01 m and 0.003 m respectively, in analogy with those of Lake Alpnach [*Lorke et al*., 2002].

The lake surface is considered as a flat surface, over which the wind stress τ_w acts. It is computed as a function of the wind speed (U_{10}) 10 m above the lake surface:

$$\tau_w = \rho_a C_{10} U_{10}^2 , \tag{8}$$

where ρ_a is the air density. The drag coefficient is calculated as

$$C_{10} = 0.0044\, U_{10}^{-1.15}, \qquad U_{10} < 1\,\mathrm{m\,s^{-1}} \tag{9}$$

$$C_{10} = (0.8 + 0.065\, U_{10}) \times 10^{-3}, \qquad U_{10} > 1\,\mathrm{m\,s^{-1}} , \tag{10}$$

with U_{10} expressed in m s^{-1}. The estimation of the drag coefficient of equation (9) was suggested by *Wüest and Lorke* [2003], whereas equation (10) is in *Wu* [1982]. Actually, we should consider the fact that the atmosphere is not neutral along the daily cycle. This may alter the velocity profile. However, data on the stability of the atmosphere were not available, and, for sake of simplification we neglected this effect on the velocity field.

Wind forcing was the only source of momentum in the lake and turbulence at the surface was triggered and sustained using a zero-mean random fluctuation with standard deviation equal to 20% of the mean value, added to the mean wind stress of equation (8).

To investigate the wind-driven circulation in Lake Ledro two scenarios were considered: the homogeneous wind case (HWC) and the inhomogeneous (IWC) one, respectively. HWC was run by using the wind direction and speed measured 2.8 m above the water surface ($U_{2.8}$) by a weather station in a platform located at point M of Figure 1a [*Boscaini et al*., 2012]. Wind data were extrapolated to 10 m using the power-law wind profile described in *Hsu et al*. [1994], assuming a neutrally stratified atmosphere and a smooth surface with a standard roughness length of 10^{-4} m, hence $U_{10} = 1.1\, U_{2.8}$ (Figure 2).

IWC was run by using the wind speed and direction simulated by WRF [*Skamarock et al*., 2008] 10 m above the lake surface, thus making a first step toward the coupled air-water simulation at local scale. The simulation performed for the present case covered the time period 16–22 January 2012, from 18:00 UTC of 15

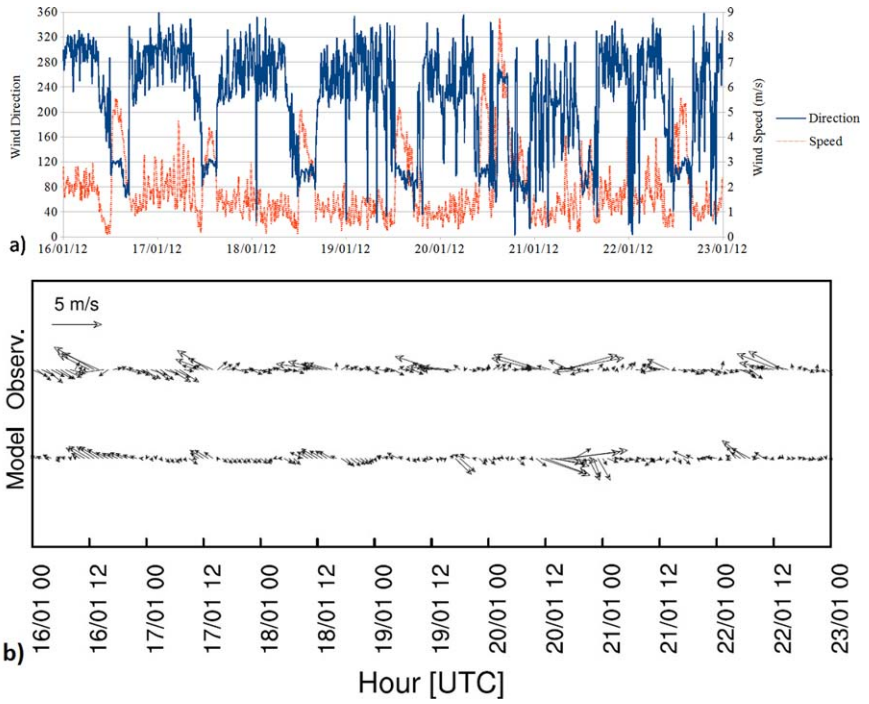

Figure 2. Wind speed and direction recorded at the platform M (see position in Figure 1a): (a) time series between 16 and 22 January 2012; (b) comparison between the wind measured at the station and the value simulated by WRF.

January 2015. The first 6 h, being spuriously affected by the initialization, were not considered for the analysis. The horizontal domain is composed of four two-way nested domains with 100x100, 91x91, 91x100, and 79x79 cells, and grid spacing of 10.8, 3.6, 1.2, and 0.4 km, respectively. For the vertical resolution, 27 levels were used. The initial and boundary conditions were supplied by the 6 hourly National Centers for Environmental Prediction (NCEP) Final Operational Global Analysis data on 1° grids.

We adopted a high-resolution topography data set with an original spatial resolution of 1″ (∼ 30 m). As regards the land use, the Corine Land Cover data set updated to 2006 (http://www.eea.europa.eu) was used for the present meteorological simulations (for further details, see *Giovannini et al.* [2014]). The simulated wind velocity was obtained in WRF on 36 equally spaced points, which were mapped on each grid point at the surface of the hydrodynamic model through a bi-harmonic spline interpolation.

The simulated period (16–22 January 2012) is characterized by the development of a periodic alternation of a weak down-valley (north-westerly) wind at night and a stronger up-valley (south-easterly) wind during afternoon, reaching a typical maximum intensity of 5–6 m s^{-1} (Figure 2). The periodicity of wind speed and direction is more evident in the first 3 days (16–18 January). In the remaining days the periodicity is less clear probably due to the influence of synoptic-scale events, more evident in the afternoon of day 5, when a strong north-westerly wind, reaching 9 m s^{-1}, blew for some hours. A comparison between the measured and simulated wind at the central platform is shown in Figure 2b. The numerical results are in a good agreement in the first 3 days. Some disagreements are present in the last 2 days of the simulation, although WRF is able to reproduce the synoptic-scale event recorded at the measurement point. The disagreement does not affect the present analysis, since the results of the meteorological simulation are used here to study the effect of the spatial inhomogeneity of the wind over the lake, rather than for having a perfect reproduction of the wind at a certain location.

In the following analysis, we first focus on turbulence characterization using the homogeneous wind field, and then we highlight the specific features originated by the spatially variable forcing. Hereafter, the average in time is denoted with $\langle . \rangle_t$, whereas the time and space average over the horizontal planes is indicated with $\langle . \rangle$. The quantity u_i' denotes the resolving fluctuations of the *i*-component of the velocity field and the quantity U_H is the module of the mean horizontal velocity field.

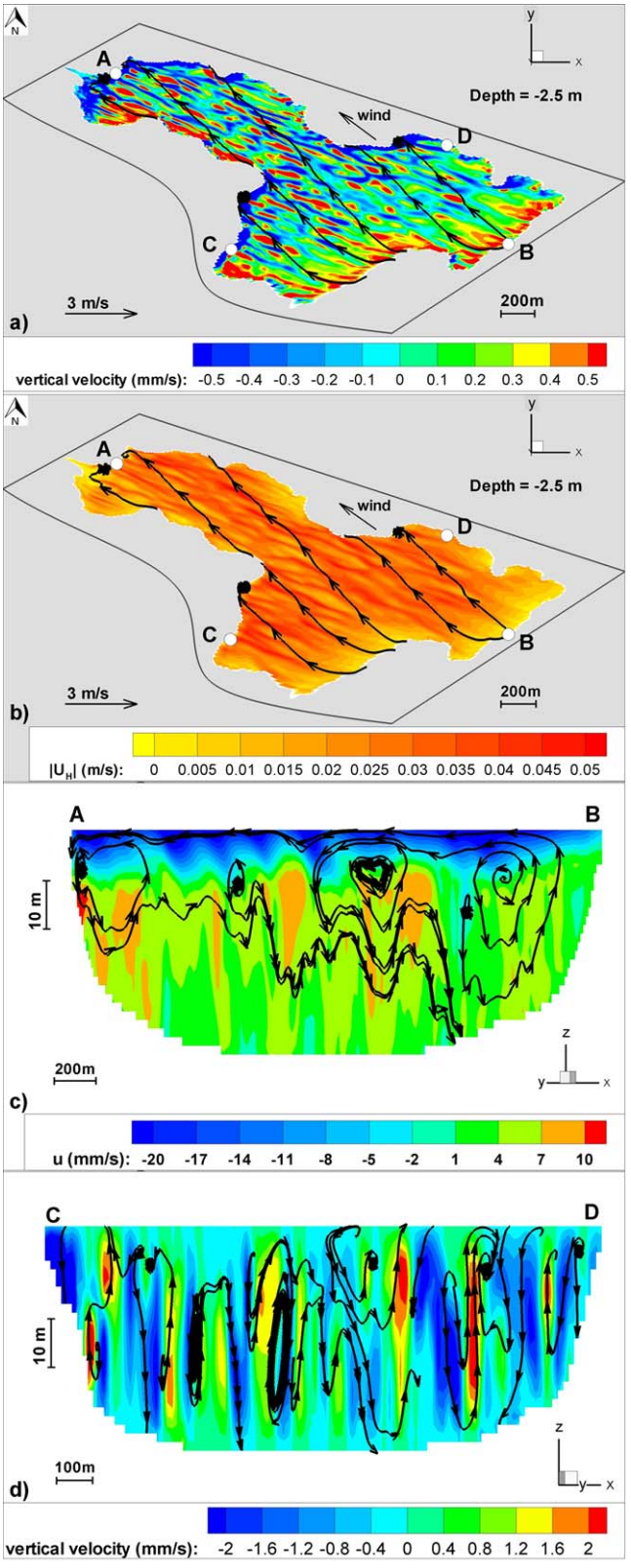

Figure 3. HWC. Snapshot of the streamtracers and instantaneous field at 13:00 of 20 January: (a) vertical, and (b) horizontal ($|U_h|$) velocity, on a horizontal plane at 2.5 m depth; (c) u in transect AB, and (d) w in transect CD.

3. Results for the Homogeneous Wind Case

Here we discuss results of a simulation carried out considering the wind of Figure 2 uniformly applied to the entire lake surface.

3.1. Velocity Field

As a representative example of the lake circulation occurring during the winter period, snapshots were taken at 13:00 of 20 January 2012, when the wind has been blowing from 135°N with an intensity of ~ 5 m s^{-1} for 4 h. This instantaneous velocity field is representative of the time period around the early afternoon when wind usually blows from south-east.

The vertical and horizontal instantaneous velocity components and streamtracers 2.5 m below the free surface are shown in Figure 3, together with vertical transects along the axes AB and CD of Figure 1b. The streamtracers indicate the presence of downwelling and upwelling areas along the windward and leeward shorelines of the lake, respectively (Figure 3a). The vertical velocity in the upwelling region is of the order of 1×10^{-3} m s^{-1} for about 6 h in the central part of the day. This gives an estimation of uprising of the order 21 meters, hence providing a physical explanation for the sudden rising of the *P. rubescens* cyanobacteria along the coasts of Lake Ledro.

The horizontal velocity is relatively low along the leeward side of the coastline in the downwelling areas (north-western coasts, see Figure 3b). The horizontal velocity in the lake interior (below 15 m of depth) is opposite to the circulation in the surface layer (Figure 3c), indicating the typical presence of a return flow and hence of a vertical circulation. The return flow is better appreciable when the wind holds the direction for a long time.

The central part of the lake is characterized by marked differences in vertical and horizontal velocities (Figure 3d), similar to stripes, suggesting the presence of wind-generated turbulent

structures, as already detected in other LES applications [*Petronio et al*., 2013; *Galea et al*., 2014], and observed in physical experiments for shallow-water wall-bounded turbulence. These superstreaks consist of rotating vortices with the axis approximately aligned with the direction of the motion and resemble the Couette streaks first presented in *Lee and Kim* [1991] and *Papavassiliou and Hanratty* [1997]. The turbulent structures have the same characteristics of the ones shown in *Tejada-Martinez and Grosch* [2007] in their case without the vortex force which is representative of the interaction between the Stokes drift and the shear current. In *Galea et al*. [2014], these structures were shown to span over a length of tens of meters in the streamwise direction and to persist for hours. These circulations enhance vertical mixing along the water column.

The typical wind-driven circulation generated during the morning (north-west $U_{10} \sim 2$ m s^{-1}), is different from the circulation generated during the afternoon because of the different direction and intensity of the wind acting on the surface. The streamtracers are tilted with respect to the wind direction because of the Coriolis effect. This has been verified repeating the simulation without the contribution of the Coriolis force and observing that, in the latter case, the instantaneous streamtracers are aligned with the wind direction (not shown). On the other hand, the dimensional analysis suggests that, although the dimension of the lake is small, the Rossby number $Ro = U_H/(Lf)$ is of the order of 0.05 (hence $\ll 1$), because of the small horizontal velocity present in the lake ($U_H \sim 10^{-2}$ m s^{-1}, $L = 2000$ m and $f = 2\Omega_3\, sen\theta = 10^{-4}$ s^{-1}, where θ is the latitude). Hence rotational effects have a role both in the deviation of the velocity vectors and in the suppression of vertical mixing, for a discussion, see *Salon and Armenio* [2011]. Also, *Toffolon* [2013] showed that Coriolis force in narrow lakes can produce a secondary circulation (in the vertical plane orthogonal to the wind direction), and not only in the so-called Ekman layer. Thus, the resulting Ekman transport involves the whole mixed layer, and produces downwelling/upwelling at the coasts. The Coriolis force becomes less important during the afternoon, when the scale of horizontal velocity is larger ($U_H \sim 0.05$ m s^{-1}, $Ro \sim 0.25$) (see Figures 3a and 3b).

3.2. Eddy Viscosities in Simplified Cases

Turbulent transport of momentum in lakes is expected to occur at a much larger rate in the horizontal direction, possibly affecting the general circulation [*Toffolon and Rizzi*, 2009]. This turbulence anisotropy is partly due to the effect of the relative shallowness of these water bodies, and partly due to the effect of stratification, which is not examined in this work.

Down-gradient turbulent transport is usually quantified through the vertical and horizontal eddy viscosity coefficients. The concept of eddy viscosity is based on the gradient-diffusion hypothesis which assumes the anisotropic Reynolds stress tensor be aligned with the mean rate of the strain tensor equation (3). Although such an assumption is somehow crude [*Kundu et al*., 2012], it is generally accepted in the scientific and engineering communities.

The vertical and horizontal eddy viscosities are expressed respectively as:

$$\nu_H = \frac{\sqrt{\widetilde{u'v'}^2}}{\sqrt{\left(\frac{\partial \widetilde{u}}{\partial y} + \frac{\partial \widetilde{v}}{\partial x}\right)^2}} + \nu_{\tau,H}\,, \tag{11}$$

$$\nu_V = \frac{\sqrt{\widetilde{u'w'}^2 + \widetilde{v'w'}^2}}{\sqrt{\left(\frac{\partial \widetilde{u}}{\partial z}\right)^2 + \left(\frac{\partial \widetilde{v}}{\partial z}\right)^2}} + \nu_{\tau,V}\,, \tag{12}$$

where $\nu_{\tau,H}$ and $\nu_{\tau,V}$ are respectively the SGS contributions of equations (4) and (5).

The symbol $\widetilde{.}$ denotes averaging performed either in time ($\langle . \rangle_t$) or in space and time ($\langle . \rangle$), according to the specific discussion of the results presented hereafter. Similarly for the SGS contributions. Note that here we calculate the eddy viscosities using the Reynolds stresses and velocity gradients obtained in an operation of postprocessing, averaging the data of our eddy resolving simulation. Standard models often use parametrization of eddy viscosity based on theory and calibration obtained for open ocean under steady or quasi-steady forcing. However, the dynamics of a small lake under a diurnal cycle of thermally-driven winds may be substantially different from the former simplified conditions. Thus, in the next section we analyze the spatial distribution of the eddy viscosity in two simplified cases: an (infinite) ocean and Lake Ledro both

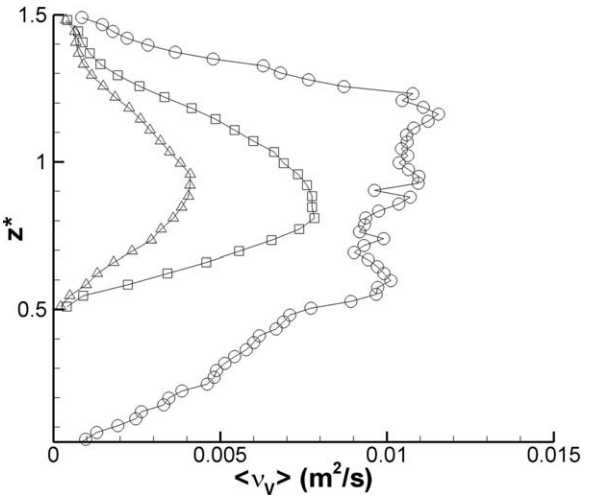

Figure 4. HWC. Vertical profile of vertical eddy viscosity $\langle \nu_V \rangle$ obtained in three cases: for an unbounded turbulent Ekman layer (solid line with circles); for the Lake Ledro under steady wind (solid line with up-pointing triangles); for the Lake Ledro under steady wind in absence of Coriolis force (solid line with squares). Unlike the rest of the paper, here the free surface is at $z^* = 1.5$.

with a spatially homogeneous steady wind, in order to evaluate the main differences between the two cases.

3.2.1. Eddy Viscosity With Steady Mean Wind

In this section, first the vertical profile of vertical eddy viscosity calculated with equation (12) is discussed in view of the results obtained in [*Zikanov et al*., 2003] for a LES of an infinite Reynolds number surface Ekman layer. Further we analyze the effect of Earth's rotation and of solid boundaries on the spatial distribution of eddy viscosities.

As a first test, we simulated the conditions for the development of an oceanic Ekman layer at $Re_E = u^*/\sqrt{f\nu} =$ with $u^* = \sqrt{\tau_w/\rho}$. The vertical profile of $\langle \nu_V \rangle$, averaged over a time window of 2 h (Figure 4) qualitatively agrees with that of *Zikanov et al*. [2003]. Specifically, in the surface layer the vertical eddy viscosity increases linearly with depth reaching its maximum at around $z* = z/L = 1.25$, where $L = u^*/f$ is the turbulent length scale. The eddy viscosity profiles obtained by *Zikanov et al*. [2003] were generated in presence of a steady wind; note that in the case of Lake Ledro, a fully developed steady flow condition would be reached after 6 days of constant unidirectional wind blowing over at the free surface. This condition is not reached in small-and medium-size lakes for two main reasons: the rapid change of the wind direction and intensity does not allow for reaching a steady state; the presence of lateral boundaries generates a circulation in the cross sections orthogonal to the wind direction [*Toffolon*, 2013].

In order to highlight the role of the boundaries and of the Coriolis force, we analyze the eddy viscosity profiles developing within the lake Ledro under homogeneous and constant wind blowing with $U_{10} = 4$ ms^{-1} for the time needed to reach the steady state. Figure 4 also shows the vertical profiles of eddy viscosities obtained in Lake Ledro with and without presence the Coriolis force. The main differences between these simulations and the oceanic case are more evident in the surface boundary layer: in bounded-domain case (Lake Ledro) the vertical eddy viscosity increases much less than in the unbounded case. Also, the Coriolis force causes a reduction of the Reynolds shear stress (not shown), thus producing lower values of vertical eddy viscosity compared to the case where Coriolis force was not simulated.

3.2.2. Spatial Distribution of Eddy Viscosity With Time-Varying Wind

Contour plots of $\langle \nu_V \rangle_t$ and $\langle \nu_H \rangle_t$ are shown in Figure 5. They were calculated over a time window of 8 h between 00:00 and 08:00 of the second day, under the wind condition measured at the meteorological station. Panels a and b show respectively the distribution of the two quantities over the vertical plane in the transect AB of Figure 1. Panels c and d show the distribution of the two quantities over horizontal planes at $z = -7.7$ m and $z = -16.3$ m.

The eddy viscosities are strongly anisotropic, with the horizontal coefficient being about 2 orders of magnitude larger than the vertical one even in the neutral conditions herein investigated. In the Surface Boundary Layer (SBL), the horizontal eddy viscosity $\langle \nu_H \rangle_t$ (Figure 5a) decreases with depth up to $z \sim -16$ m, then it grows reaching a maximum at $z \sim -40$ m. The vertical eddy viscosity $\langle \nu_V \rangle_t$ (Figure 5b) is very small at the surface and it increases in the SBL reaching its maximum at $z \sim -28$ m.

Interestingly, the two quantities exhibit substantial inhomogeneity along the horizontal planes. In the lake interior (e.g., at $z = -16.3\,m$) the horizontal eddy viscosity $\langle \nu_H \rangle_t$ is much larger far from the coastline (Figure 5c) where the values of the horizontal velocity gradients are smaller. Conversely, the vertical eddy viscosity $\langle \nu_V \rangle_t$ is larger along the shoreline, due to the presence of the boundary layers associated to upwelling and downwelling regions, with high values of the Reynolds shear stresses ($\langle u'w' \rangle_t$ and $\langle v'w' \rangle_t$).

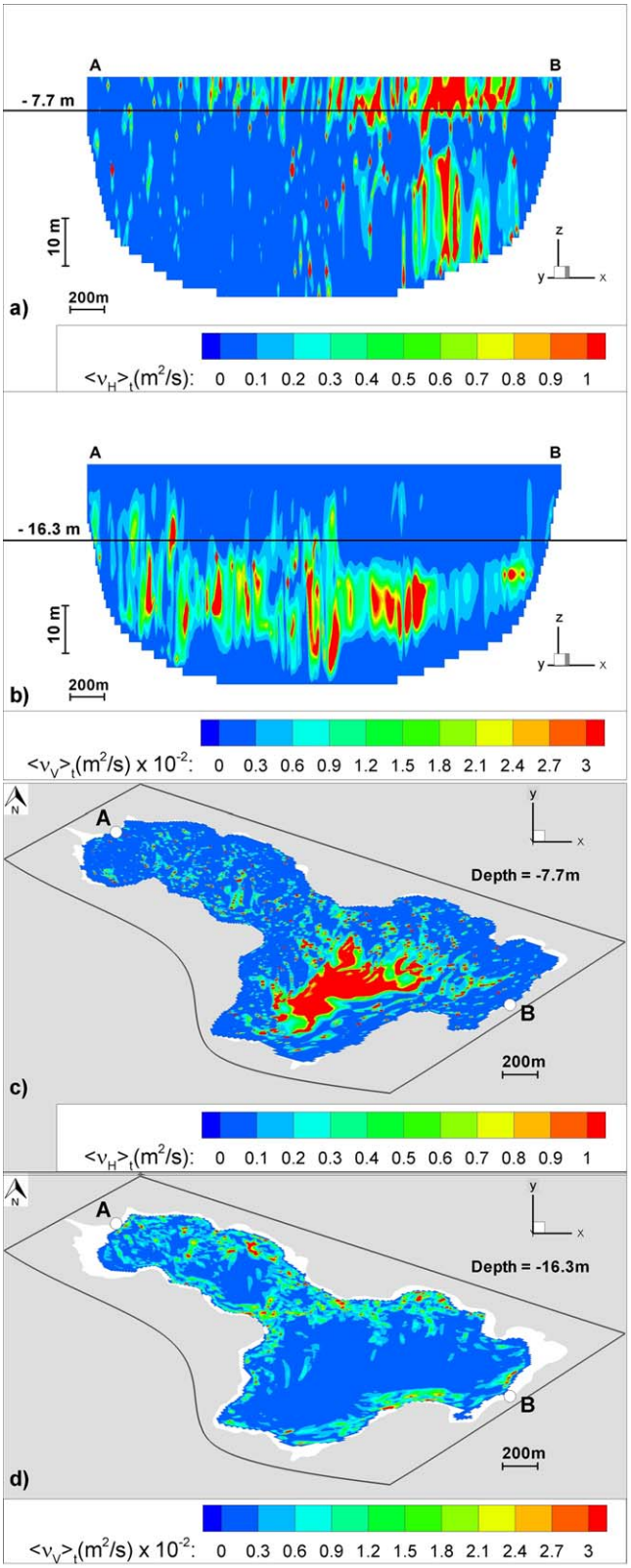

Figure 5. HWC. Eddy viscosities obtained averaging over 8 h between 00:00 and 08:00 of 17 January. Contour plots of: (a) $\langle \nu_H \rangle_t$ over the transect AB of Figures 1a; (b) $\langle \nu_V \rangle_t$ over the transect AB of Figure 1a; (c) $\langle \nu_H \rangle_t$ on a horizontal plane at $z = -7.7$ m; (d) $\langle \nu_V \rangle_t$ on a horizontal plane at $z = -16.3$ m.

In Figure 6a, we report the vertical profiles of the space-time averaged values of $\langle \nu_H \rangle$ and $\langle \nu_V \rangle$. Differently from those shown in Figure 4, here the quantities are obtained over the time window of 8 h as described above. Unlike the case with the steady mean wind where $\langle \nu_H \rangle$ remains constant along the depth (not shown), in this case it is roughly constant down for the first 5 m and then it decreases reaching its minimum value at around $z = -15$ m, due to a rapid reduction of the Reynolds shear stresses (Figure 6b) showing the presence of a minimum-stress plane. The vertical eddy viscosity $\langle \nu_V \rangle$ increases with the distance from the free surface down to $z \sim -30$ m similarly to the case shown in Figure 4. For larger depths, $\langle \nu_V \rangle$ first increases rapidly because of the decrease of the vertical gradients of the horizontal velocities and successively decreases due to the rapid decrease of the Reynolds shear stress (Figure 6c). The behavior of the vertical eddy viscosity in the bottom region is representative of the weakness of the bottom boundary layer as we will discuss later on in the paper.

Finally in Figure 7 we show the space-time averaged eddy viscosities $\langle \nu_V \rangle$ and $\langle \nu_H \rangle$ along the 6 days simulated. The quantity $\langle \nu_V \rangle$ is always at its climax in the core of the water basin, and its intensity is modulated according to the wind stress. The maximum of the horizontal eddy viscosity $\langle \nu_H \rangle$ is close to the free surface and large values of this quantity propagate up to the deep layers in case of large wind stress.

3.3. Turbulent Kinetic Energy and Dissipation Rate

The Turbulent Kinetic Energy (TKE) is a measure of the intensity of velocity fluctuations within the water body:

$$\widetilde{TKE} = \frac{1}{2}\left(\widetilde{u'u'} + \widetilde{v'v'} + \widetilde{w'w'}\right) \tag{13}$$

It is mainly confined in the resolved scales and the SGS contribution is generally low. The resolved-scale dissipation rate of TKE is:

$$\widetilde{\epsilon_r} = -2\nu\,\widetilde{s_{ij}s_{ij}}\,, \quad s_{ij} = \frac{1}{2}\left(\frac{\partial u_i'}{\partial x_j} + \frac{\partial u_j'}{\partial x_i}\right). \tag{14}$$

However, since most of the dissipative scales of motion are confined in the subgrid, the total ϵ was estimated adding to ϵ_r the rate of energy transferred from the filtered motion to the residual one ($P_{SGS} \equiv -\tau_{ij}S_{ij}$), which is equal to the SGS dissipation rate ϵ_{SGS} of the turbulent energy for high Reynolds numbers [*Pope*, 2000]. According to the eddy viscosity model of equation (3),

$$\widetilde{\epsilon_{SGS}} = \widetilde{P_{SGS}} = -\widetilde{\tau}_{ij}\widetilde{S}_{ij} = 2\widetilde{\nu}_\tau \widetilde{S}_{ij}\widetilde{S}_{ij}\,, \tag{15}$$

hence,

$$\widetilde{P_{SGS}} = 2\widetilde{\nu}_{\tau,H}(\widetilde{S}_{11}^2 + 2\widetilde{S}_{22}^2 + \widetilde{S}_{12}^2) + 2\widetilde{\nu}_{\tau,V}(2\widetilde{S}_{13}^2 + \widetilde{S}_{33}^2 + 2\widetilde{S}_{23}^2). \tag{16}$$

The total dissipation rate of TKE is expressed as $\widetilde{\epsilon} = \widetilde{\epsilon_r} + \widetilde{\epsilon_{SGS}}$.

As for the eddy viscosity analysis, $\langle TKE \rangle$ and $\langle \epsilon \rangle$ were calculated between 10:00 and 12:00 of the day 3 and between 14:00 and 16:00 of day 5, when the wind is characterized by $\langle \tau_w \rangle \sim 0.002 N/m^2$ and $\langle \tau_w \rangle \sim 0.02 N/m^2$ respectively; they are reported in Figures 8 and 9. High values of $\langle TKE \rangle$ are detected close to the free surface, a 'minimum-stress' plane is present at $z \sim -16$ m and small values are observed at the bottom of the lake. This is an evidence of the fact that the wind is the main source of turbulence, the latter nearly absent at the bottom of the lake, consistently with the results of the eddy viscosity analysis.

The total dissipation rate is composed of two terms. The contribution of the resolved scales is of the order of 10^{-14}–10^{-15} W kg^{-1}, suggesting that most of the dissipation occurs at the subgrid scales, as expected due to the resolution herein employed. The averaged dissipation rate ranges between 10^{-9} W kg^{-1} and 10^{-6} W kg^{-1}; it peaks in the SBL, decreases exponentially in the top 15 m and reaches the minimum value at the bottom of the lake. The typical increase of ϵ in the Bottom Boundary Layer (BBL) is not present in our case, due to the absence of stratification and seiches [*Wüest et al.*, 2000]. On the other hand, we can estimate the intensity of the boundary layer induced in the Lake Ledro by seiches, taking advantage of the knowledge of the tidal-induced boundary layer theory (see *Salon et al.* [2007], and references therein). Based on available data, a typical free-surface seiche in the Lake Ledro has been estimated as having a period of $T_s = 2L_s/\sqrt{(gH_s)} \sim 240$ s, considering a horizontal length $L_s = 2500$ m, with a typical amplitude

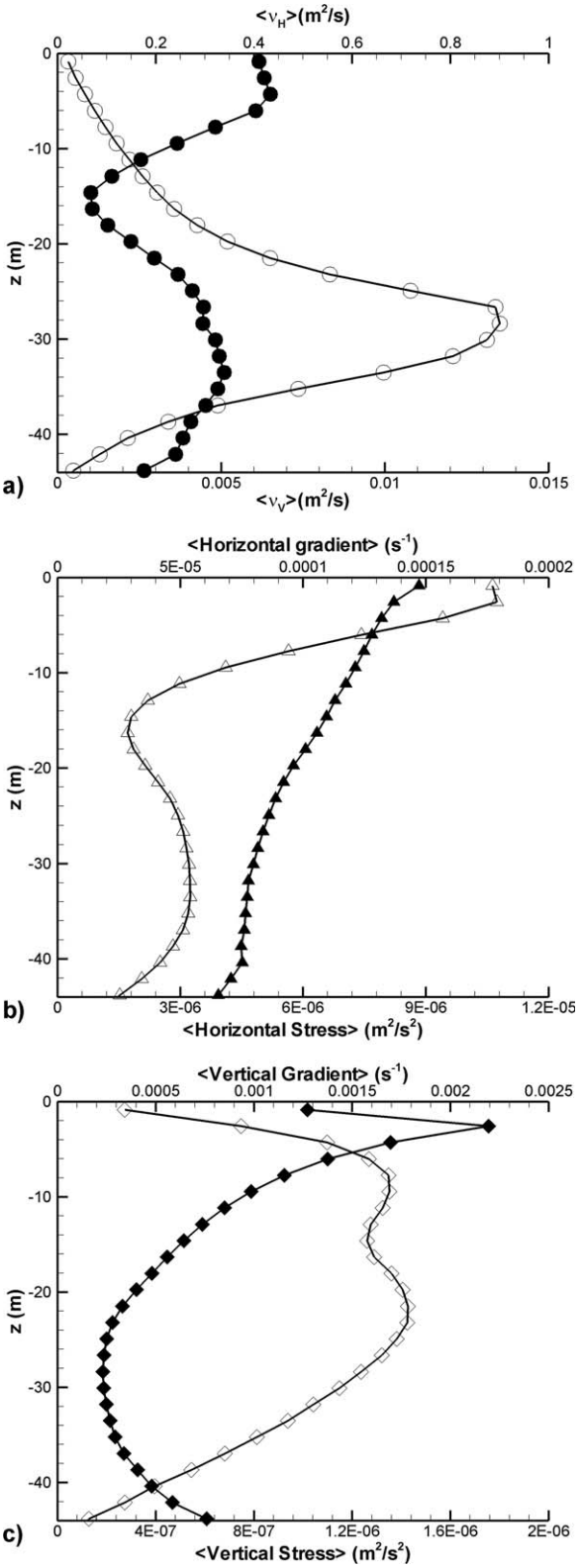

Figure 6. HWC. Vertical profiles of space-time quantities averaged over 8 h: (a) $\langle \nu_V \rangle$ (solid line with white circles) and $\langle \nu_H \rangle$ (solid line with black circles); (b) horizontal stresses (solid line with white up-pointing triangles) and horizontal gradients (solid line with black up-pointing triangles); (c) vertical stress along z axis (solid line with white diamond), and vertical gradients along z axis (solid line with black up-pointing triangles). Stresses and gradients correspond respectively to numerator and denominator in equations (11) and (12).

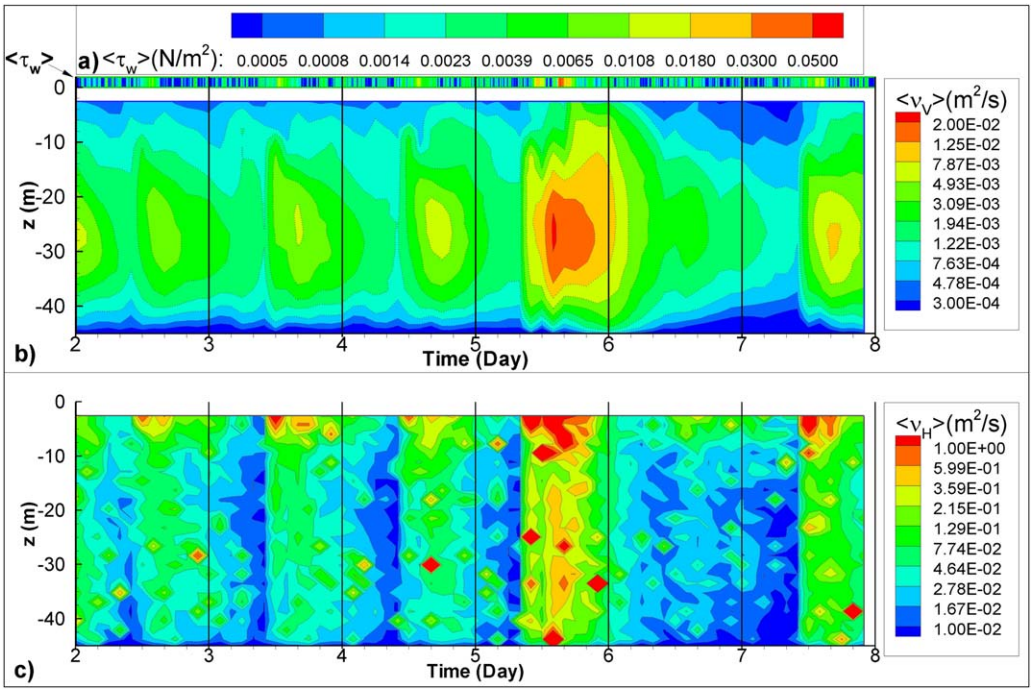

Figure 7. HWC. Vertical profiles of space-time quantities averaged over 2 h along the latter 6 days of simulation: (a) $\langle \tau_w \rangle$; (b) $\langle \nu_V \rangle$; and (c) $\langle \nu_H \rangle$.

$H_s = 0.04$ m. With these values we can calculate a horizontal pressure gradient associated to the hydrostatic unbalance between the two sides of the lake having an amplitude of $\Pi_0 = 0.16$ N m^{-3}. Assuming a sinusoidal oscillation of the horizontal pressure gradient $\Pi = \Pi_0 \sin(2\pi t/T_s)$, since in the outer layer of the BBL $\partial U/\partial t = -\Pi$, we can estimate the amplitude of the free-stream motion at the bottom surface as $U_s = T_s \Pi_o/(2\pi\rho) = 6.1\times10^{-3}$ m s^{-1}. The BBL intensity can be estimated based on the value of $Re = U_s^2 T_s/(2\pi\nu) \sim 1400$ smaller than the value 1.5×10^5 at which the boundary layer moves into a transitional intermittent regime [*Salon et al.*, 2007]; thus the BBL induced by the free surface seiche is very weak and in the laminar regime. Hence, the typical increase of ϵ in the BBL is not expected to occur due to free-surface seiches, rather it may be caused by large amplitude internal waves due to the presence of stable stratification. This is the subject of an upcoming study.

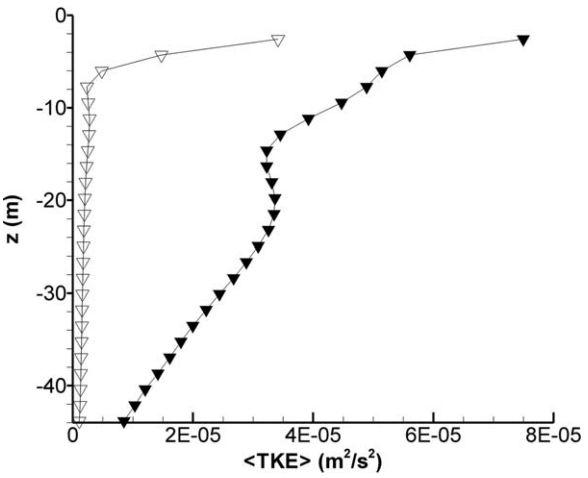

Figure 8. HWC. Vertical profile of the space-time $\langle TKE \rangle$ averaged over 2 h between 10:00 and 12:00 of the day 3 (solid line with white down-pointing triangles) and between 14:00 and 16:00 of the day 5 (solid line with black down-pointing triangles) respectively.

Figure 10 shows the evolution along the latter 6 days simulated of the vertical profiles of 2 h space-time averaged $\langle TKE \rangle$ and $\langle \epsilon \rangle$. The evolution of the flow starting from the quiescent state takes approximately 1 day; for this reason the first day of simulation is not discussed.

They appear substantially modulated according to the intensity of the wind stress. $\langle TKE \rangle$ is approximately in phase with the wind stress at the free surface, peaking a bit earlier than the wind intensity and approximately in phase with the change of wind direction which may constitute ad additional source of turbulence. $\langle TKE \rangle$ exhibits the largest values in the free-surface region, as expected due to the fact that the wind stress is the only source of

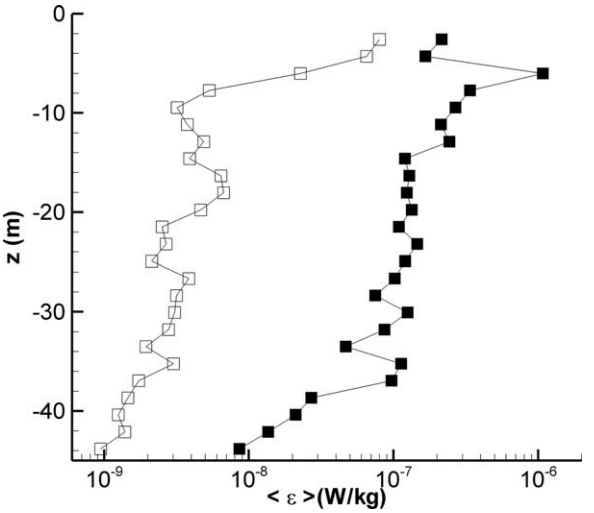

Figure 9. HWC. Vertical profile of the space-time $\langle\epsilon\rangle$ averaged over 2 h between 10:00 and 12:00 of the day 3 (solid line with white squares) and between 14:00 and 16:00 of the day 5 (solid line with black squares) respectively.

turbulence. It propagates toward the deeper layers with a time delay of the order of 8 h, appearing a bit reduced when the wind intensity increases. This indicates that the large scales of motions, represented by the large vortices present in the water basin are not able to transfer turbulent fluctuations very rapidly along the water depth. When the wind increases the turbulence is enhanced and is able to transfer at a faster rate fluctuations toward the bottom.

The space-time averaged $\langle\epsilon\rangle$ behaves similarly to $\langle TKE\rangle$ indicating the presence of equilibrium turbulence along the water column, thus suggesting that the unsteady term of the transport equation of TKE may plays a minor role. Overall the analysis suggest that the turbulent time scales are much smaller that the time scale of the wind forcing.

4. Results for the Inhomogeneous Wind Case

In this section, we analyze the circulation generated by an inhomogeneous wind stress, provided by the WRF model, with the aim of highlighting the main differences with respect to the Homogeneous Wind Case (HWC).

The main differences with the previous HWC is that inhomogeneity may create zones of relevant horizontal divergence in the free surface region and also that the local orography may produce zones of either very low or high wind speed. The latter effect is quantified by the root mean square deviations (RMS) of the

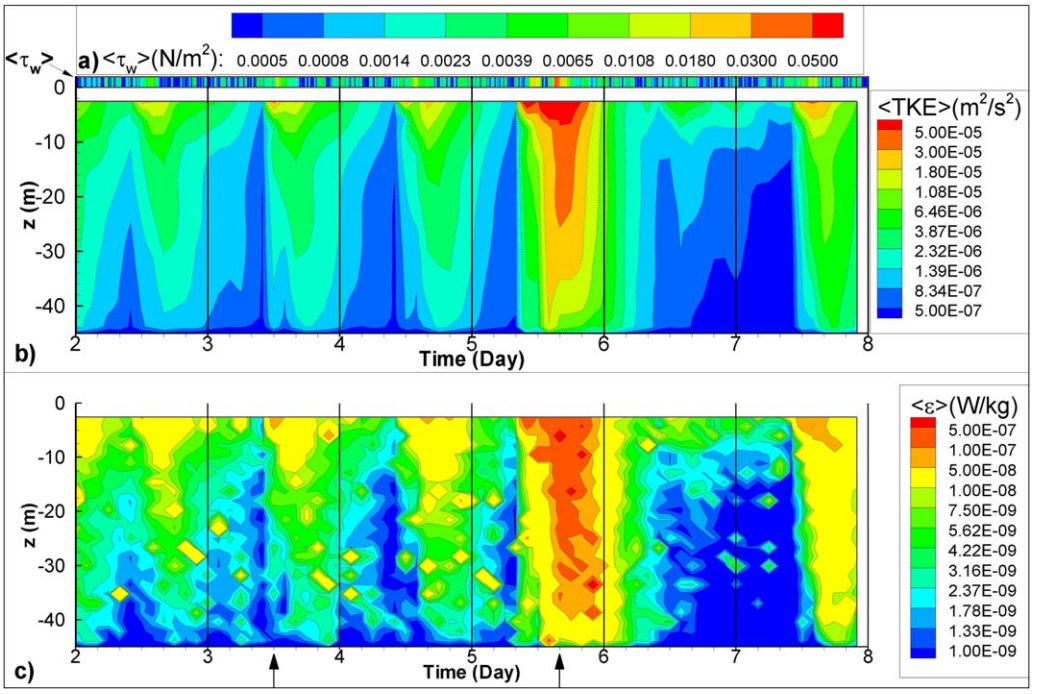

Figure 10. HWC. Vertical profiles of space-time quantities averaged over 2 h along the latter 6 days of simulation: (a) $\langle\tau_w\rangle$; (b) $\langle TKE\rangle$; and (c) $\langle\epsilon\rangle$. The vertical profile of the $\langle TKE\rangle$ and $\langle\epsilon\rangle$ at the time indicated in by the arrows in c) are reported in Figures 8 and 9.

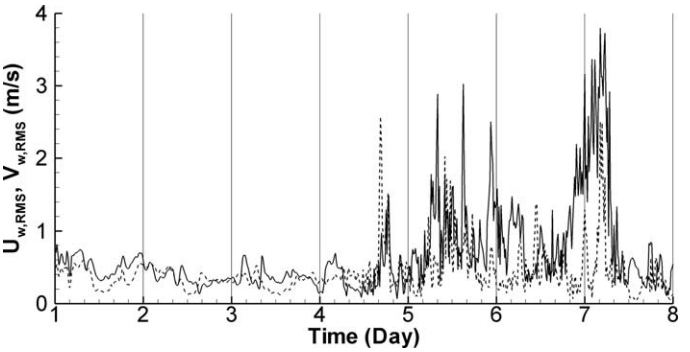

Figure 11. IWC. Root Mean Square (RMS) of U_w (solid line) and V_w (dotted line) over the lake between day 1 (16 January) and day 7 (22 January).

two horizontal components U_w and V_w of the wind velocity with respect to their space averaged values (Figure 11).

The first 3 days are characterized by low inhomogeneity and light breeze. On the contrary, the last 4 days are characterized by larger wind stress and substantial inhomogeneity: peaks of the RMS of U_w and V_w occur in the afternoon of day 4 of the simulation, during day 5, and in the early morning of day 7.

The evolution along the latter 6 days, of the vertical profile of the 2 h space-time averaged eddy viscosities is in Figure 12. With respect to the HWC we note that the vertical eddy viscosity is less regular (periodic) and overall smaller in the first days of light breeze and low inhomogeneity. However, if we compare the quantities made nondimensional with Hu^* (not shown) where H is the depth of the lake, we observe that this nondimensional quantity is overall larger for the inhomogeneous case. This means that the eddy viscosity resulting from a certain wind stress is larger in the inhomogeneous case. This is even more true in the last days of the simulations, characterized by the synoptic events giving rise to large inhomogeneity. The same discussion holds for the horizontal eddy viscosity. Even if the dimensional values in the case of light breeze appear larger in HWC, the nondimensional values are always larger in the IWC.

The same behavior holds for the evolution along the 6 days of the vertical profiles of the 2 h space-time averaged TKE and its dissipation rate (Figure 13). In presence of light wind the dimensional values appear larger for HWC (compare Figure 10 with Figure 13). However, we have looked at the quantities made nondimensional with u^{*2} and u^{*3}/H respectively, in order to quantify the turbulent kinetic energy and its

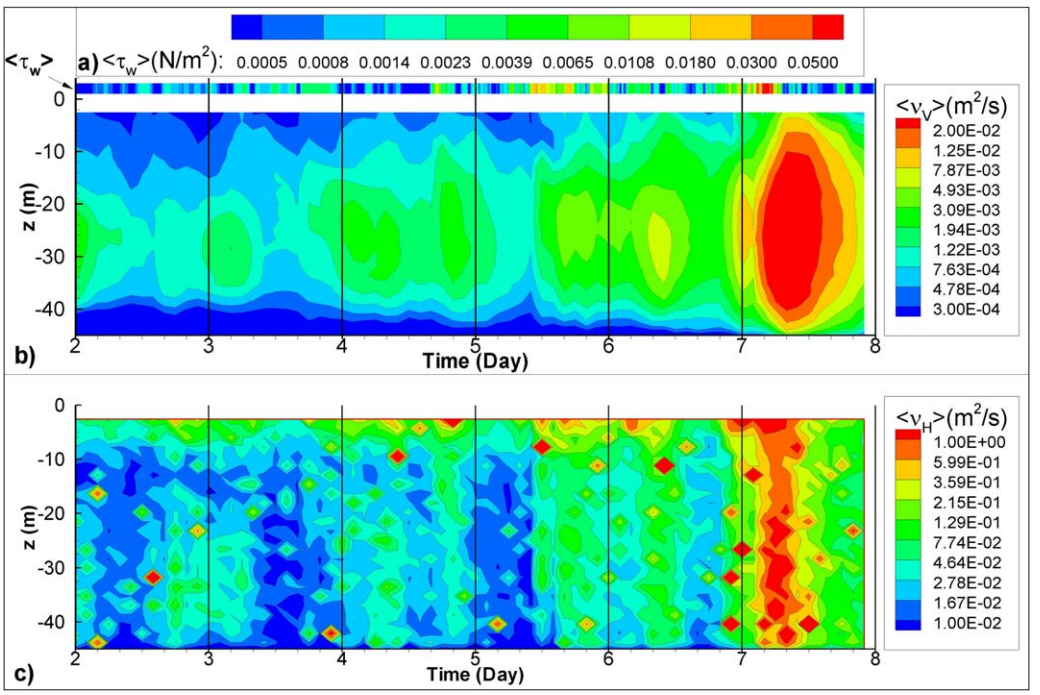

Figure 12. IWC. Vertical profiles of space-time quantities averaged over 2 h along the latter 6 days of simulation: (a) $\langle \tau_w \rangle$; (b) $\langle \nu_V \rangle$, and (c) $\langle \nu_H \rangle$.

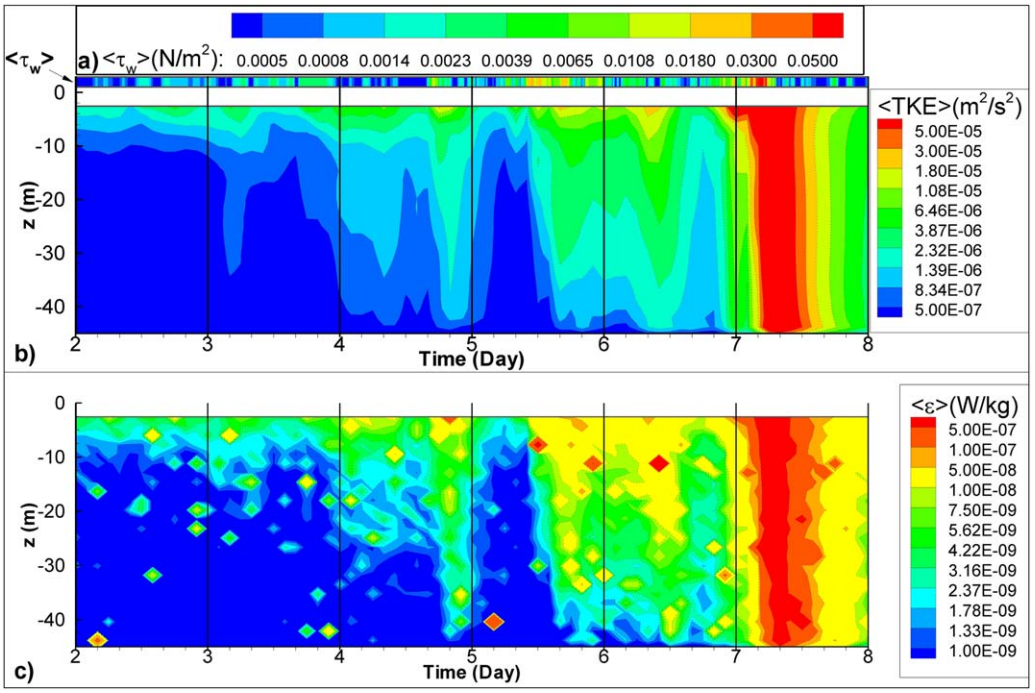

Figure 13. IWC. Vertical profiles of space-time quantities averaged over 2 h along the latter 6 days of simulation: (a) $\langle \tau_w \rangle$; (b) $\langle TKE \rangle$, and (c) $\langle \epsilon \rangle$.

dissipation rate associated to a certain intensity of wind stress. As for the eddy viscosities, the non dimensional quantities (not shown) appear always larger for the IWC. Finally, in presence of large inhomogeneity, (last day of the simulation) the comparison between Figure 10 and Figure 13 shows that dimensional quantities appear larger for the IWC, suggesting that spatial variation of the wind stress may provide an additional source of mixing. The phase-lag between the wind stress and the two quantities $\langle TKE \rangle$ and $\langle \epsilon \rangle$ is not appreciably different from the HWC. The phase-lag between the values of the two quantities at the surface and the correspondent values at the bottom of the lake appears a bit reduced and of the order of 6 h suggesting that inhomogeneity may affect the response time of turbulence in the lake interior.

One of the two effects of wind inhomogeneity is the occurrence of nonzero horizontal divergence. Positive values indicate local upwelling events, the opposite is true for negative values. This is clearly shown in Figure 14 where we show the instantaneous wind field 2.8 m above the water surface and the horizontal divergence of the velocity field below the free surface. These effects are even more intense in correspondence of the most relevant wind stress events acting on the surface of the lake (not shown). In general, the inhomogeneity of the wind represents an additional source of mixing, not present when the wind blows homogeneously on the surface of the lake. This lends justification to the discussion of eddy viscosities, turbulent kinetic energy and its dissipation rate reported above.

5. Conclusions

An eddy-resolving model (LES-COAST) was applied to study the hydrodynamics and the turbulent structures of a lake as a whole. We studied Lake Ledro, a peri-alpine lake in northern Italy for three main reasons: The lake suffers from metalimnetic blooms of the cyanobacteria *P. rubescens*, which appears at the lake surface during winter in neutrally stratified conditions; its own dimensions are suitable for a high-resolution simulation; it is a significant example of a lake where orographic features affect the wind distribution over the lake surface.

A period of 7 days in January was simulated referring to typical neutrally stratified conditions. Wind forcing was reproduced using two different conceptual methodologies: first we considered the case of spatially homogeneous wind field with values obtained from measurements at a weather station; successively, we

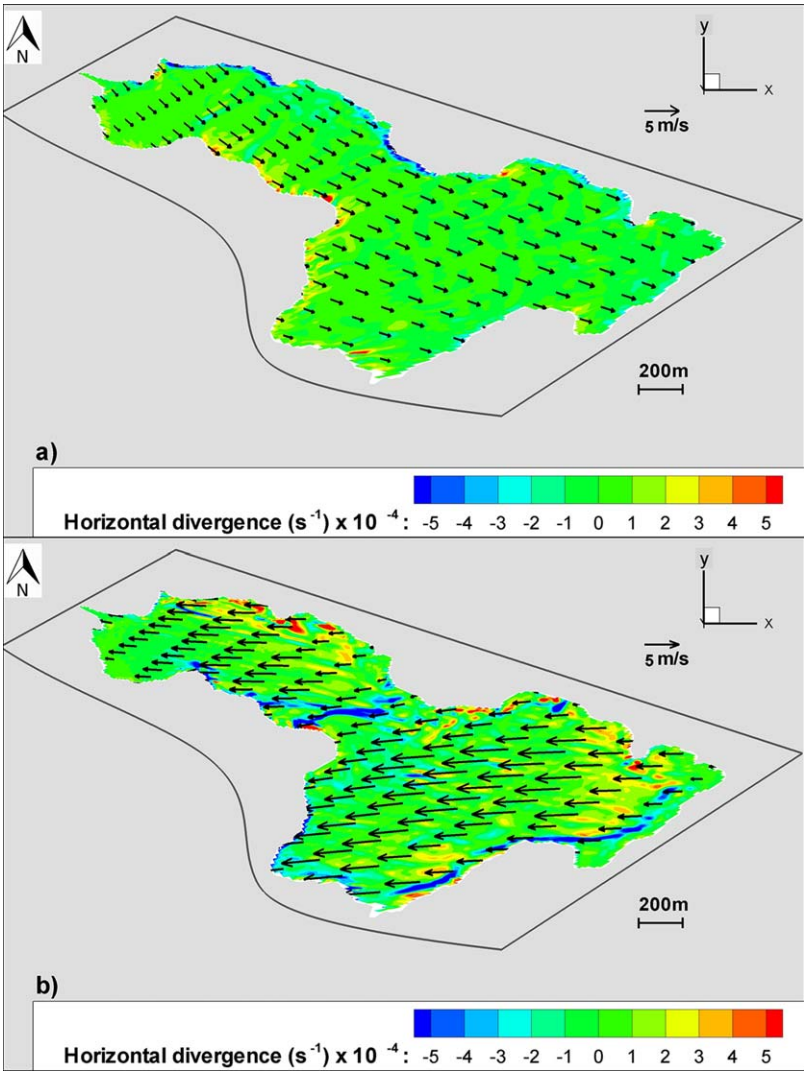

Figure 14. IWC. Contour plot at z=-0.8m of depth of the divergence of the horizontal velocity field together with vectors of the wind field 2.8 m above the surface of the Lake: (a) small inhomogeneity at 19:30 of the day 3, (b) large inhomogeneity at 23:15 of day 6.

considered an inhomogeneous wind field obtained through a 'local-scale' meteorological simulation, carried out using an atmospheric model (WRF).

Overall, the analysis shows that:

1. The overall hydrodynamics is characterized by the development of velocity field in the surface boundary layer, which inverts its own direction approximately at a depth of 10 m.
2. The Coriolis force plays a role in the dynamics by tilting to the right the velocity field with respect to the wind direction and by decreasing the eddy viscosities. This is particularly true under light breeze conditions, when the surface current is weak.
3. Upwelling and downwelling regions are recognized along the leeward and windward coastline respectively. The estimation of the vertical uprising associated to the vertical velocity in the upwelling region, may give explanation to the sudden appearance of the cyanobacteria at the lake surface in neutrally stratified conditions.
4. No substantial bottom boundary layer activity is present for three main reasons: the time window over which the wind acts steadily along a direction is not large enough to allow for the development of a turbulent bottom boundary layer; The estimation of the surface seiches shows that they are too weak to

produce a significant turbulent boundary layer at the bottom of the lake; The absence of large amplitude internal waves associated to stable stratification, the latter not considered in the present work.

5. In agreement with classic literature, the horizontal eddy viscosity is some orders of magnitude larger than the vertical one. When looking at their spatial distribution, they exhibit inhomogeneous behavior over the horizontal planes. The horizontal eddy viscosity is larger in the interior of the lake than close to the coastline, whereas the vertical eddy viscosity is larger along the coasts due to the presence of the boundary layer. The vertical profiles of the space-time averaged eddy viscosities were also discussed. The horizontal one evidences the presence of a 'minimum-stress plane' just below the SBL; the vertical one has its own climax in the core of the water basin. It substantially differs from that obtained for an hypothetical unbounded surface Ekman layer (the typical ocean case) because of the presence of the lateral boundaries of the lake and because of the absence of a steady mean wind able to develop a steady-state flow field. Also, the study shows that, under significant wind unsteadiness, the vertical eddy viscosity appears different from the theoretical profile obtained in idealized steady conditions.
6. Peculiar superstreaks are reproduced in the interior of the lake. Their lifetime is of the order of hours, they span over the entire depth of the lake and are elongated along the direction of motion. This kind of structures was recently visualized in laboratory experiments of shallow-water wall-bounded turbulence as well as in simulations of Couette flows. They supply vertical mixing in the water column.
7. The turbulent kinetic energy and its dissipation rate, are roughly in phase with the wind forcing. They propagate toward the bottom with a phase lag of about some hours with respect to the values at the free surface. Also, they propagate down to the bottom with the same rate indicating the presence of equilibrium turbulence even under the unsteady conditions herein studied.
8. The role of a spatially inhomogeneous wind stress was assessed by imposing the wind field simulated by the meteorological model, thus accounting for the sheltering and channeling effects of the surrounding steep orography. We measured the degree of inhomogeneity calculating the RMS deviations of the wind distribution over the lake. Under light breeze conditions, and in presence of small inhomogeneity, the dimensional values of eddy viscosities, TKE and its dissipation rate are more sensitive to the wind intensity and appear slightly affected by inhomogeneity. However, when these quantities are made non dimensional, thus considering them with respect to the wind forcing, it clearly appears that inhomogeneity supplies more mixing. This is particularly true under synoptical events where inhomogeneity is large. Wind inhomogeneity seems to reduce the response time of turbulence within the lake, transferring fluctuations at a faster rate compared to HWC. Although this discussion of wind inhomogeneity might be of general use, we point out that it holds for the case examined in the present work under neutral conditions and more research is needed.

A study of stratified condition is ongoing and is the topic of a successive paper.

Acknowledgments

Measurements were collected by Foundation Edmund Mach (FEM) within the project 'Quantificazione dei carichi di nutrienti ed analisi del trasporto nel lago di Ledro' funded by Provincia Autonoma di Trento (Italy). We gratefully thank Nico Salmaso and Adriano Boscaini (FEM) for kindly providing lake bathymetry and wind data. The present research has been partially funded by 'Progetto Bandiera RITMARE', action SP3-WP4-AZ3-U7 and SP5-WP4-AZ4-UO06 and by the University of Trieste, 'Project FRA 2013, Modellistica numerica e sperimentale di fenomeni di erosione localizzata in alvei fluviali'. The data and files necessary to reproduce the simulations, are available from the authors upon request (santomarco31@gmail.com). The simulations were carried out using computational facilities procured through the European Regional Development Fund, project ERDF-080 "Supercomputing Laboratory for the University of Malta" (http://www.um.edu.mt/research/scienceeng/erdf_080). The authors wish to acknowledge Prof. V. Nikora for useful discussion.

References

Arrilaga, J. A., C. Yague, M. Sastre, and C. RomÀn-Cascòn (2016), A characterisation of sea-breeze events in the eastern Cantabrian coast (Spain) from observational data and WRF simulations, *Atmos. Res.*, *181*, 265–280.

Barbato, G. (1977), Note idrobiologiche sul Lago di Ledro, *Ann. Mus. Civ. St. Nat. Brescia*, *14*, 92–109.

Boscaini, A., F. Brescancin, and N. Salmaso (2012), Progetto di ricerca per lo sviluppo dei fattori fisico-chimici che regolano lo sviluppo del cianobatterio Planktothrix Rubescens nel lago di Ledro [in Italian], Fondazione E. Mach - Istituto Agrario di S. Michele a/A, Dipartimento Agroecosistemi Sostenibili E Biorisorse, S. Michele all'Adige, Italy.

Burchard, H., et al. (2008), Observational and numerical modelling methods for quantifying coastal ocean turbulence and mixing, *Prog. Oceanogr.*, *76*, 399–442.

D'Alelio, D., and N. Salmaso (2011), Occurrence of an uncommon Planktothrix (Cyanoprokaryota, Oscillatoriales) in a deep lake south of the Alps, *Phycologia*, *50*, 379–383.

Dittko, K. A., M. P. Kirkpatrick, and S. W. Armfield (2013), Large Eddy Simulation of complex sidearms subject to solar radiation and surface cooling, *Water Res.*, *47*, 4918–4927.

Galea, A., M. Grifoll, F. Roman, M. Mestres, V. Armenio, A. Sanchez-Arcilla, and L. Zammit Mangion (2014), Numerical simulation of water mixing and renewals in the Barcelona harbour area: The winter season, *Environ. Fluid Mech.*, *14*, 1405–1425.

Giovannini, L., D. Zardi, M. De Franceschi, and F. Chen (2014), Numerical simulations of boundary-layer processes and urban-induced alterations in an Alpine valley, *Int. J. Climatol.*, *34*, 1111–1131.

Giovannini, L., L. Laiti, D. Zardi, and M. De Franceschi (2015), Climatological characteristics of the Ora del Garda wind in the Alps, *Int. J. Climatol.*, *35*, 4103–4115.

Hsu, S. A., E. A. Meindl, and D. B. Gilhousen (1994), Determining the Power-Law Wind-Profile exponent under near-neutral stability conditions at sea, *J. Appl. Meteorol.*, *33*, 757–765.

Kundu, P. K., I. M. Cohen, and D. R. Dowling (2012), *Fluid Mechanics*, Academic, Waltham, Mass.

Laiti, L., D. Zardi, M. De Franceschi, G. Rampanelli, and L. Giovannini (2014), Analysis of the diurnal development of a lake-valley circulation in the Alps based on airborne and surface measurements, *Atmos. Chem. Phys.*, *14*, 9771–9786.

Laval, B., J. Imberger, B. R. Hodges, and R. Stoker (2003), Modeling circulation in lakes: Spatial and temporal variations, *Limnol. Oceanogr. Methods*, *48*, 983–994.
Lee, M. J., and J. Kim (1991), The structure of turbulence in a simulated plane Couette flow, in *Proceedings of 8th Symposium on Turbulent Shear Flows*, vol. 1, Munich, Germany.
Lorke, A., L. Umlauf, T. Jonas, and A. Wüest (2002), Dynamics of turbulence in low- speed oscillating bottom-boundary layers of stratified basins, *Environ. Fluid Mech.*, *2*, 291–313.
Mironov, D., A. Terzhevik, G. Kirillin, T. Jonas, J. Malm, and D. Farmer (2002), Radiatively driven convection in ice-covered lakes: Observations, scaling, and a mixed layer model, *J. Geophys. Res.*, *107*(C4), 3032, doi:10.1029/2001JC000892.
Papanastasiou, D. K., D. Melas, and I. Lissaridis (2010), Study of wind field under sea breeze conditions; an application of WRF model, *Atmos. Res.*, *98*, 102–117.
Papavassiliou, D. V., and T. J. Hanratty (1997), Interpretation of large-scale structures observed in a turbulent plane Couette flow, *Int. J. Heat Fluid Flow*, *18*, 55–69.
Petronio, A., F. Roman, C. Nasello, and V. Armenio (2013), Large Eddy Simulation model for wind-driven sea circulation in coastal areas, *Nonlinear Processes Geophys.*, *20*, 1095–1112.
Piomelli, U. (1999), Large-eddy simulation: Achievements and challenges, *Prog. Aerospace Sci.*, *35*, 335–362.
Podsetchine, V., and G. Schernewski (1999), The influence of spatial wind inhomogeneity on flow patterns in a small lake, *Water Res.*, *15*, 3348–3356.
Pope, S. B. (2000), *Turbulent Flows*, Cambridge Univ. Press, Cambridge, U. K.
Rampanelli, G., D. Zardi, and R. Rotunno (2004), Mechanisms of up-valley winds, *J. Atmos. Sci.*, *61*, 3097–3111.
Roman, F., V. Armenio, and J. Fröhlich (2009a), A simple wall layer model for Large Eddy Simulation with immersed boundary method, *Phys. Fluids*, *21*, 101701.
Roman, F., E. Napoli, B. Milici, and V. Armenio (2009b), An improved immersed boundary method for curvilinear grids, *Comput. Fluids*, *38*, 1510–1527.
Roman, F., G. Stipcich, V. Armenio, R. Inghilesi, and S. Corsini (2010), Large eddy simulation of mixing in coastal areas, *Int. J. Heat Fluid Flow*, *31*, 327–341.
Rubbert, S., and J. Köngeter (2005), Measurements and three-dimensional simulations of flow in a shallow reservoir subject to small-scale wind field inhomogeneities induced by sheltering, *Aquat. Sci.*, *67*, 104–121.
Rueda, F. J., S. G. Schladow, S. G. Monismith, and M. T. Stacey (2005), On the effects of topography on wind and generation of currents in a large multi-basin lake, *Hydrobiologia*, *532*, 139–151.
Salmaso, N., G. Morabito, F. Buzzi, L. Garibaldi, M. Simona, and R. Mosello (2006), Phytoplankton as an indicator of the water quality of the deep lakes south of the Alps, *Hydrobiologia*, *563*, 167–187.
Salon, S., and V. Armenio (2011), A numerical investigation of the turbulent Stokes–Ekman bottom boundary layer, *J. Fluid Mech.*, *684*, 316–352.
Salon, S., V. Armenio, and A. Crise (2007), A numerical investigation of the Stokes boundary layer in the turbulent regime, *J. Fluid Mech.*, *570*, 253–296.
Sander, J., A. Simon, T. Jonas, and A. Wüest (2000), Surface turbulence in natural waters: A comparison of large eddy simulations with microstructure observations, *J. Geophys. Res.*, *105*, 1195–1207.
Sarkar, S., and V. Armenio (2013), Direct and large eddy simulation of environmental flows, in *Handbook of Environmental Fluid Dynamics*, vol. 2, edited by H. J. S. Fernandog, pp. 283–299, CRC Press, Boca Raton, Fla.
Scalo, C., L. Boegman, and U. Piomelli (2013), Large-eddy simulation and low-order modeling of sediment-oxygen uptake in a transitional oscillatory flow, *J. Geophys. Res. Oceans*, *118*, 1926–1939, doi:10.1002/jgrc.20113.
Serafin, S., and D. Zardi (2010), Structure of the atmospheric boundary layer in the vicinity of a developing upslope flow system: A numerical model study, *J. Atmos. Sci.*, *67*, 1171–1185.
Skamarock, W. C., J. B. Klemp, J. Dudhia, D. O. Gill, D. M. Barker, M. G. Duda, X.-Y. Huang, W. Wang, and J. G. Powers. (2008), A description of the advanced research WRF version 3, *NCAR Tech. Note TN-475+STR*, p. 125, Mesoscale and Microscale Meteorol. Div., Natl. Cent. for Atmos. Res., Boulder, Colo.
Smagorinsky, J. (1963), General circulation experiments with the primitive equations, *Mon. Weather Rev.*, *91*, 99–120.
Tejada-Martinez, A. E., and C. E. Grosch (2007), Langmuir turbulence in shallow water: Part 2. Large-eddy simulation, *J. Fluid Mech.*, *576*, 63–108.
Toffolon, M. (2013), Ekman circulation and downwelling in narrow lakes, *Adv. Water Resour.*, *53*, 76–86.
Toffolon, M., and G. Rizzi. 2009. Effects of spatial wind inhomogeneity and turbulence anisotropy on circulation in an elongated basin: A simplified analytical solution, *Adv. Water Resour.*, *32*, 1554–1566.
Wu, J. (1982), Wind-stress coefficient over sea surface from breeze to hurricane, *J. Geophys. Res.*, *87*, 9704–9706.
Wüest, A., and A. Lorke (2003), Small-scale hydrodynamics in lakes, *Annu. Rev. Fluid Mech.*, *35*, 373–412.
Wüest, A., G. Piepke, and D. C. Van Senden (2000), Turbulent kinetic energy balance as a tool for estimating vertical diffusivity in wind-forced stratified waters, *Limnol. Oceanogr.*, *45*, 1388–1400.
Zikanov, O., D. N. Slinn, and M. R. Dhanak (2003), Large-eddy simulations of the wind-induced turbulent Ekman layer, *J. Fluid Mech.*, *495*, 343–368.